

Rational Selection of Transition Metal Co-Dopant in Sulfur-Doped Titanium Dioxide †

Edgar Clyde R. Lopez ^{1,2} 

¹ Nanotechnology Research Laboratory, Department of Chemical Engineering, University of the Philippines, Quezon City 1101, Philippines; edgarclydelopez09@gmail.com

² Chemical Engineering Department, Adamson University, Manila 1000, Philippines

† Presented at the 2nd International Electronic Conference on Processes: Process Engineering—Current State and Future Trends (ECP 2023), 17–31 May 2023; Available online: <https://ecp2023.sciforum.net/>.

Abstract: This paper investigates the general trends in the structural, electronic, and optical properties of anatase TiO₂ photocatalysts co-doped with transition metals and sulfur. We attempt to rationalize co-dopant selection by employing molecular dynamics and density functional theory calculations. The structural properties of the first-row transition metal co-dopants were determined. TM-TiO₂ and TM/S-TiO₂ were structurally stable, with minimal changes in their lattice parameters, cell volume, density, and XRD profiles relative to pristine TiO₂. However, only Fe and Mn among the first-row transition metals are thermodynamically favorable, i.e., their substitutional energies are lower relative to pristine TiO₂. Intermediate energy levels (IELs) are formed during the co-doping of transition metals and sulfur on TiO₂. In particular, Fe and Co form two IELs between the VBM and CBM, resulting in improved optical properties, especially in the visible-light region, which are mainly attributed to the unsaturated nonbonding transition metal d orbitals and the half-filled Ti–O bonding orbitals. On the other hand, Cu and Ni form three IELs close to each other due to the M–O anti-bond orbitals, half-filled p orbitals of S, and the Ti–S anti-bonding orbitals. These IELs in co-doped systems can serve as “stepping stones” for photogenerated electrons, facilitating easier charge mobility. Among the investigated co-doped systems, Fe/S-TiO₂ was shown to be the most promising for photocatalytic applications.

Keywords: molecular dynamics; density functional theory; titanium dioxide; co-doping; photocatalysis



Citation: Lopez, E.C.R. Rational Selection of Transition Metal Co-Dopant in Sulfur-Doped Titanium Dioxide. *Eng. Proc.* **2023**, *37*, 15. <https://doi.org/10.3390/ECP2023-14699>

Academic Editor: Antoni Sánchez

Published: 17 May 2023



Copyright: © 2023 by the author. Licensee MDPI, Basel, Switzerland. This article is an open access article distributed under the terms and conditions of the Creative Commons Attribution (CC BY) license (<https://creativecommons.org/licenses/by/4.0/>).

1. Introduction

Titanium dioxide, a widely available metal oxide semiconductor, has been used by many researchers for various applications since the first reports of Fujishima and Honda [1] on UV-induced chemical reactions on its surface. Among its common uses are the photocatalytic degradation of organics in water [2,3], the treatment of volatile organic compounds (VOCs) in the air [4–6], and photoelectrochemical water splitting and hydrogen production [7–9], among others.

Despite the extensive use of titanium dioxide in the literature, its commercial applications are minimal due to various key challenges in its feasible large-scale use that remain unaddressed. Among the issues identified based on a surface science perspective [10], the most important issues are bandgap engineering to alter the optical properties toward the visible light region, thus enabling solar-driven photocatalytic reactions and charge transport engineering to suppress if not wholly arrest electron–hole recombination.

Doping titanium dioxide is the most popular method for narrowing its bandgap. It involves the addition of one or more atoms, called the dopant, within the crystal lattice of titanium dioxide to intentionally alter its electronic and optical properties. Doping can either be substitutional or non-substitutional (interstitial and surface doping). Various dopants have been used and are generally categorized as cationic or anionic dopants.

Cationic doping is more widely studied; common cationic dopants are noble metals [11], transition metals [12], and rare earth metals [13]. Doping with a transition metal ion increases the formation of Ti^{3+} ions, enhancing photocatalytic activity. More Ti^{3+} states may cause more oxygen defects, facilitating efficient oxygen adsorption on the titania surface. The formation of O_2^- upon oxygen chemisorption requires a surface defect site which can be enhanced via transition metal ion doping. Since the redox energy states of many transition metal ions lie within the bandgap states of TiO_2 , substituting metal ions into the TiO_2 introduces an intraband state close to the CB or VB edge, inducing visible light absorption at sub-bandgap energies [14]. Previous first-principles calculations revealed that they introduce intermediate energy levels (IELs) that were previously absent in pristine TiO_2 due to the delocalization of the $3d$ or $4d$ states of the transition metals; sometimes these states hybridize with the Ti's $3d$ and O's $2p$ states, thus altering its electronic structure and improving its visible light absorption ability by narrowing the bandgap [15–17].

On the other hand, anionic dopants such as nitrogen [18], sulfur [19], and halogens [20,21] were also used to enhance visible light photocatalysis to extend the optical absorption edge of TiO_2 . Because anions are less electronegative than O, substitutional doping causes the anionic p -states to be pushed up out of the TiO_2 valence band into the bandgap [10]. In the case of nitrogen doping, the decrease in the conduction band minimum (CBM) and the increase in the valence band minimum (VBM) causes a narrower bandgap, the extent of which is dependent upon the dopant concentration [22]. Nonmetal ion doping is a promising way to avoid the deteriorating thermal stability of the TiO_2 lattice [14].

Despite the effectiveness of doping in extending the photocatalytic range of TiO_2 to the visible light region, various factors should be considered to ensure that it will translate to the desired photoactivity. Issues with cationic doping, such as induced thermal instability and enhanced electron–hole recombination when the metals act as either photogenerated electron traps, such as in p-type doping, or photogenerated hole traps, such as in n-type doping, could be detrimental to the photocatalytic activity of TiO_2 [23]. In the case of anionic doping, post-processing annealing could lead to a reduced dopant concentration [24].

The co-doping of TiO_2 with two or more elements was carried out by some researchers [25–27] to address the concerns regarding individual cationic or anionic doping. The strong interaction between these dopants within the TiO_2 matrix alters the charge carrier transfer–recombination dynamics and shifts the bandgap absorption to the visible region. The coupling of one dopant with a second has been proposed to enable a reduction in the number of carrier recombination centers via the proposed charge equilibrium mechanism and to enhance the visible light absorbance by increasing the solubility limits of the dopants [14]. In our previous work, we co-doped copper and sulfur to titanium dioxide and showed a significant increase in its photocatalytic activity when the material was used to degrade organic pollutants in water [28].

Although co-doping a transition metal with S enhanced photocatalytic activity, selecting a co-dopant is not trivial. For example, which trends do the bandgap changes follow in the transition metal series? What criteria for selecting a transition metal for co-doping with S will lead to an enhanced photoactive catalyst? A detailed analysis of the electronic structure change based on co-doping different transition metals with N could provide insight into the underlying physical origin of the photocatalytic activity. Therefore, this paper describes an investigation of a first-row transition metal series co-doped with S, using molecular dynamics (MD) calculations and density functional theory (DFT) to elucidate the effects of co-doping on the structural and electronic properties of TM/S (TM represents first-row transition metals) co-doped TiO_2 to reveal the atomic relationship between the band structure and the origin of the enhanced photocatalytic activity.

2. Computational Details

TiO_2 exhibits three crystal phases, among which the anatase phase is the most photocatalytically active. Anatase TiO_2 has a tetragonal structure with a symmetry group of $I4_1/AMD$ and lattice parameters of $a = b = 3.776 \text{ \AA}$ and $c = 9.486 \text{ \AA}$. Doping systems were

constructed using a 48-atom anatase supercell with a $2 \times 2 \times 1$ repetition. The (TM and S) co-doped configurations were constructed by replacing one oxygen atom with a sulfur atom and a Ti atom with a TM atom. The atomic ratio of TM to Ti was 0.0625, close to the value used in many experimental studies. The supercell with co-doped TM and S is shown in Figure 1.

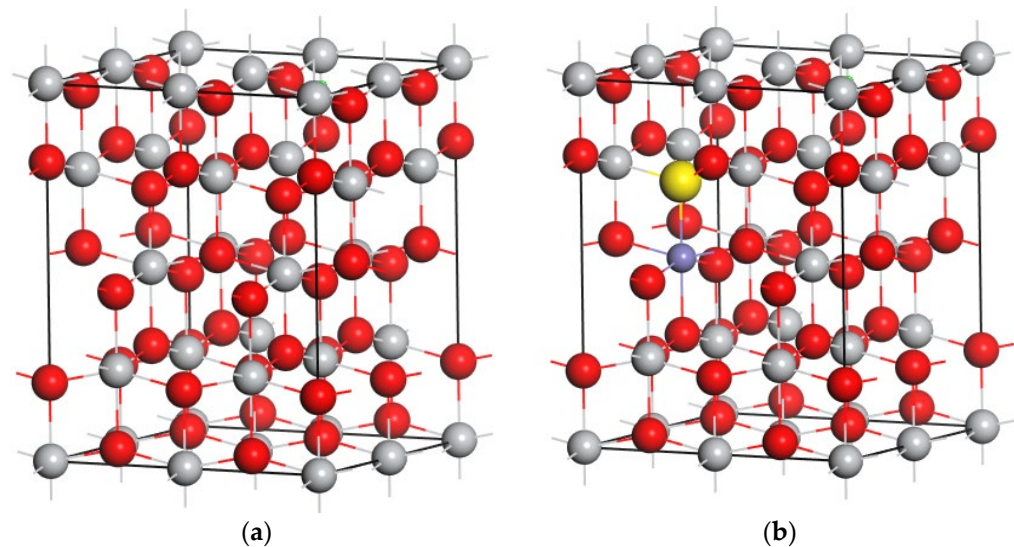


Figure 1. Tetrahedral structure of: (a) pristine TiO_2 , (b) TM/S- TiO_2 . Color coding: Ti = gray, O = red, S = yellow, and TM = purple.

For the rational selection of co-dopants, molecular dynamics calculations were performed using the Forcite module of Materials Studio using the Universal forcefield (UFF). A geometry optimization of the supercells was achieved using a cascade of the steepest descent and the adjusted basis set Newton–Raphson (ABNR) and quasi-Newton methods with the total energy, maximum force, maximum stress, and maximum displacement tolerance values set to 2×10^{-5} eV per atom, $0.001 \text{ eV \AA}^{-1}$, 0.001 GPa , and $1 \times 10^{-5} \text{ \AA}$, respectively. The Ewald summation method was used for the electrostatic and van der Waals interactions with an Ewald accuracy of 1×10^{-5} eV.

Molecular dynamics calculations were then carried out with the optimized supercells, using the NPT ensemble at 298 K and 1 atm. Pressure and temperature control were achieved using the Berendsen barostat with a decay constant of 0.1 ps and the Nosé–Hoover thermostat with a Q ratio of 0.1. The simulation was allowed to proceed for 5 ns at a 1.0 fs timestep for 5 million steps; frames were saved every 100 steps. Again, the Ewald summation method was used for the electrostatic and van der Waals interactions with an Ewald accuracy of 1×10^{-5} eV.

Spin-polarized DFT calculations were performed using the CASTEP module of Materials Studio with the GGA-PBE functional. Electron–ion interactions were modeled using ultrasoft pseudo-potentials in the Vanderbilt form. The wave functions of the valence electrons were expanded through a plane wave basis set to a cutoff energy of 400 eV. The Monkhorst–Pack scheme with a $4 \times 4 \times 3$ K-point grid generated k-points for reciprocal space sampling. The convergence threshold for self-consistent iterations was set to 5×10^{-6} eV. In the geometry optimization process, the energy change, maximum force, maximum stress, and maximum displacement tolerance values were set to 2×10^{-5} eV per atom, 0.05 eV \AA^{-1} , 0.1 GPa , and 0.002 \AA , respectively.

Co-doping with S and a transition metal is expected to alter the oxidation states of the Ti atoms surrounding the dopant. The oxidation state of the doped transition metal also depends on its local environment. As such, the DFT + U method was adopted to describe the strong on-site Coulomb repulsion. The DFT + U method has been employed to describe the electronic structures more accurately, as well as the strong on-site Coulomb

repulsion among the localized transition metal $3d/4d$ electrons. The spherically averaged Hubbard parameter U describes the increase in energy caused by placing an extra electron at a particular site, and the parameter J (1 eV) represents the screened exchange energy. The effective Hubbard parameter, $U_{\text{eff}} = U - J$, which accounts for the on-site Coulomb repulsion for each affected orbital, is the only external parameter required in this approach. In this work, the corresponding transition metal oxide bandgap was used to determine the suitable Hubbard U parameters used in the calculations.

3. Results and Discussion

3.1. Transition Metal and Sulfur Co-Doped TiO_2 : Insights from Molecular Dynamics

The co-doping of TiO_2 with a transition metal has been used to improve its optical properties to make visible-light-driven photocatalysis a reality. However, as mentioned previously, dopant selection is usually non-trivial. Investigating the effects of various dopants on the photocatalytic activity of TiO_2 is wasteful and experimentally time-consuming. Herein, we demonstrate the use of molecular dynamics calculations to rationalize the selection of transition metals for co-doping with sulfur in TiO_2 . An MD simulation was carried out, and the time-averaged structural properties, i.e., lattice constants, density, and total energy, are tabulated in Tables S1 and S2 for both the TM- TiO_2 and TM/S- TiO_2 , respectively. The periodic trend in these properties across the first-row transition metal series of the periodic table is shown in Figure S1.

In general, doping TiO_2 with TMs leads to an overall cell contraction except for Mn, for which cell expansion was observed. In the case of TM/S- TiO_2 , cell contraction occurred for all TM/S- TiO_2 except for Sc/S- TiO_2 . It appears that transition metals can cause a structural rearrangement of the cell, leading to volume changes. Meanwhile, an investigation of the cell density revealed that the densities of TM- TiO_2 and TM/S- TiO_2 increase from left to right across the first-row transition metals. This may be due to the increasing atomic weight of the TMs coupled with decreases in cell volume across the periodic table. An analysis of the structural parameters showed that all TM- TiO_2 and TM/S- TiO_2 have relative density differences within $\pm 3\%$ with respect to pristine TiO_2 and $\pm 3\%$ with respect to S- TiO_2 , respectively. Moreover, all TM- TiO_2 and TM/S- TiO_2 have relative cell volume changes within $\pm 2\%$ with respect to pristine TiO_2 and S- TiO_2 , respectively. This is good because we want to have only small changes in the structure of the TiO_2 as it translates into the structural stability of the TM- TiO_2 and TM/S- TiO_2 materials. In this discussion, we neglect the presence of titanium and oxygen vacancies, which have been reported to reduce the energy cost of incorporating the dopant into the host lattice.

To further investigate the structural character of the TM- TiO_2 and TM/S- TiO_2 , their respective X-ray diffraction profiles were simulated using the Forcite Module of Materials Studio and are shown in Figure S2 for TM- TiO_2 and Figure S3 for TM/S- TiO_2 . The degree of crystallinity for each system was estimated using the VAMP module of Materials Studio and is summarized in Table S3 for TM- TiO_2 and Table S4 for TM/S- TiO_2 . According to the generated results, the XRD profiles of the TM- TiO_2 and TM/S- TiO_2 are not significantly different from that of pristine TiO_2 . This is expected because during substitutional doping, we are only replacing (an) atom(s) with (an)other atom(s), unlike in interstitial doping, in which the dopants are distributed within the void spaces of the crystal. As such, it is highly unlikely for new XRD peaks to occur in substitutional doping because the appearance of new peaks occurs when the crystal is non-homogeneous, i.e., there are two or more crystal phases within the material of interest. The most prominent peak observed in the simulated XRD profile of pristine TiO_2 occurred at $2\theta = 25.5^\circ$, corresponding to the (101) plane of anatase. This is consistent with what we have observed experimentally. This is also the most catalytically active surface of TiO_2 , as shown in many studies in the literature. It was observed that doping causes a shift in the (101) plane peak to higher 2θ values by around $\pm 0.15^\circ$ for TM- TiO_2 and $\pm 0.10^\circ$ for TM/S- TiO_2 , with corresponding changes in the peak intensity. This is expected because substituting the Ti atom with TM and substituting the O

atom with the S atom causes a structural rearrangement, breaking the crystal symmetry. This can potentially impact the properties and stability of TiO₂.

Substitutional doping involves the breakage and formation of bonds, which requires substitutional energy. This energy barrier should be overcome to synthesize the doped TiO₂ successfully. To understand how TM and TM/S doping affects the energetics of the TiO₂ formation, the total energies of TM-TiO₂ and TM/S-TiO₂ were plotted with varying TMs. The results are shown in Figure S2e,f. In general, replacing an atom within the crystal is energetically unfavorable. Therefore, we want to have a dopant or co-dopant that can readily be incorporated within the crystal structure of TiO₂ so that thermodynamic constraints will not be an issue. Our results showed that among the first-row transition metals, only Mn and Fe are thermodynamically favorable with respect to substitutional doping into TiO₂. Mn and Fe can easily be incorporated into the anatase crystal structure without extreme conditions during their synthesis. This stabilization could be due to the formation of the closed-shell structures of these doped systems, which make the generation of oxygen or titanium vacancies unnecessary. This is crucial in reducing the formation of point defects during doping, which has beneficial effects with respect to the recombination rate and consequently on the photocatalytic properties of the material [15]. Although other TM-TiO₂ and TM/S-TiO₂ are deemed energetically unfavorable based on our MD calculations, it does not necessarily mean that these structures cannot be obtained or are unstable. These structures can be obtained at high temperatures which provide the necessary driving force to overcome the energy barrier of TM-TiO₂ and TM/S-TiO₂ formation.

3.2. Late Transition Metal and Sulfur Co-Doped TiO₂: Insights from Density Functional Theory

Based on the above discussion, we have shown that Mn/S-TiO₂ and Fe/S-TiO₂ are the most favorable structures among the first-row transition metal series. However, we still do not know whether these structures would result in enhanced photocatalytic activity under visible light illumination, which is the ultimate goal of materials scientists seeking to make solar photocatalysis a reality.

As such, we also performed density functional theory calculations to model the electronic structures and determine the optical properties of the late TM/S-TiO₂ (TM = Fe, Co, Ni, and Cu). For comparison, the band structures of the late TM-TiO₂ are shown in Figure S4, including that of S-TiO₂. Substitutional TM/S co-doping causes additional partially occupied S-2*p* states and TM-3*d* states in the band gap of TiO₂. Two distinct impurity energy levels (IELs) in the electronic structure were observed for Fe/S-TiO₂ and Co/S-TiO₂. The first IEL occurs just above the Fermi level at around 0.6–0.7 eV, followed by another IEL at around 1.5–2.3 eV. Fe/S-TiO₂ and Co/S-TiO₂ have widely spaced IELs, which can be attributed to the bonding orbital of the Ti–O bonds next to the doped atom. These IELs can serve as “stepping stones” for absorbing low energy photons and promoting electrons from the highest occupied molecular orbital, i.e., the valence band, to the first IEL and then to the second IEL and lastly to the lowest unoccupied molecular orbital, i.e., the conduction band.

On the other hand, three additional IELs were observed for Ni/S-TiO₂ and Cu/S-TiO₂. The first IEL occurs just above the Fermi level at around 0.6–0.8 eV, followed by another IEL at around 0.8–1.1 eV. The last IEL is seen at around 1.1 eV to 1.8 eV. Ni/S-TiO₂ and Cu/S-TiO₂ have closely spaced IELs. Although these lead to significant bandgap reductions, these “concentrated” regions of IELs may not effectively offer the advantage of “stepping stones” for low-energy photons [29].

For Fe and Co, the IELs induced by dopants can be divided into two categories: (i) the unsaturated, nonbonding *d* orbitals (mainly *d*_{xy}, *d*_{yz}, and *d*_{xz}) of the doped transition metal located below the CBM, and (iii) the bonding orbitals of the Ti–O bond next to the doped transition metal, located close to the Fermi level. In the case of Ni and Cu, the IELs are divided into three parts: (i) states originating from the M–O anti-bonding orbitals, located right below the CBM; (ii) states originating from the S *p*_z orbital, located in the middle of

the gap region; and (iii) states originating from electron transfer-induced S–Ti anti-bonding orbitals, located right above the Fermi level [15].

The optical absorption spectra of the late TM/S-TiO₂ were also determined from DFT calculations. As shown in Figure S5, pure anatase mainly absorbs light in the ultraviolet region. Upon introducing dopants, the absorption edges are shifted to the visible-light region. For TM/S-TiO₂, the optical spectra were altered, particularly in the case of Fe/S-TiO₂ and Co/S-TiO₂. This supports our hypothesis that IELs distributed between the bandgap of TiO₂ are more effective at absorbing photons than the concentrated IELs observed in Ni/S-TiO₂ and Cu/S-TiO₂. Again, in a TiO₂ system, co-doping transition metals and sulfur led to the formation of IELs between the VBM and CBM which offer “stepping stones” for absorbing low energy photons and promoting electrons from the VBM to the IELs and then to the conduction band.

3.3. Rational Selection of Co-Dopants

Designing, fabricating, and tailoring the physicochemical and optical properties of TiO₂ is indispensable to utilizing a large fraction of the solar spectrum and realizing the indoor applications of this photocatalyst [14]. Unfortunately, the selection of co-dopants is usually arbitrary—experimentalists simply select a combination of dopants without clearly understanding why they might work. This is frustrating based on the perspective materials scientists. As such, this paper attempted to rationalize the selection of transition metal co-dopants by combining computational tools, specifically molecular dynamics and the density functional theory, to guide researchers in rationally selecting appropriate co-dopants.

There are several factors that we must consider in the selection of a suitable co-dopant. First, co-doping TiO₂ should lead to a visible-light-active photocatalyst. Hence, the resulting co-doped TiO₂ should have a bandgap of less than 3.2 eV to be optically active under solar illumination. After performing DFT + U calculations, we showed that co-doping TiO₂ with transition metals and sulfur leads to visible-light-active photocatalysts. Second, the resulting photocatalyst should be structurally and thermally stable. Upon performing molecular dynamics calculations, it was also shown that at the low dopant levels considered in this study, the resulting co-doped systems are structurally stable, as evidenced by only small changes in their densities, lattice constants, cell volumes, and XRD profiles relative to that of pristine TiO₂. Third, substitutional co-doping should be thermodynamically favorable, i.e., the substitutional energy of the co-doped systems should be lower than that of the pristine TiO₂ to enable its synthesis without requiring tremendous amounts of energy. Based on our molecular dynamics study, only iron and manganese are deemed energetically favorable among the transition metal choices.

A volcano plot is shown in Figure S6 to summarize our findings, focusing on late-transition metals. Herein, we show that even though Cu/S-TiO₂ has the narrowest bandgap (and is thus the most photoactive among the late transition metal co-doped systems), it has a very high level of energy relative to that of pristine TiO₂. This means it might require severe conditions to overcome the thermodynamic energy barrier to synthesize this photocatalyst. Therefore, among the late transition metals, Fe/S-TiO₂ seems to be the most attractive choice among the co-doped systems because it is structurally stable, thermodynamically favorable, and visible-light active.

4. Conclusions

Herein, transition metal and sulfur co-doped TiO₂ systems were investigated to rationalize the selection of co-dopants for photocatalytic applications. Molecular dynamics calculations showed that TM-TiO₂ and TM/S-TiO₂ are structurally stable, with minimal changes in their lattice parameters, cell volumes, densities, and XRD profiles relative to pristine TiO₂. However, not all transition metals lead to thermodynamically favorable doped and co-doped systems. Our calculations have shown that only iron and manganese, among the first-row transition metals, are thermodynamically favorable, i.e., their substitutional energies are lower than the substitutional energy of pristine TiO₂. Further DFT + U

calculations on late transition metals and sulfur co-doped TiO₂ revealed that intermediate energy levels (IELs) are formed during co-doping. For example, Fe and Co form two IELs between the VBM and CBM, improving optical properties, especially in the visible-light region. These IELs are mainly due to the unsaturated nonbonding transition metal *d* orbitals and the half-filled Ti–O bonding orbitals. On the other hand, Cu and Ni form three IELs close to each other due to the M–O anti-bond orbitals, half-filled *p* orbitals of S, and Ti–S anti-bonding orbitals. These IELs in co-doped systems can serve as “stepping stones” which aid the photogenerated electrons in jumping from the VBM to these IELs and then to the CBM. This facilitates easier charge mobility and thus possibly arrests electron–hole recombination, a major issue for semiconductor photocatalyst systems. Therefore, the location of these IELs was of paramount importance and affected the optical properties of the co-doped TiO₂. Among the investigated co-doped systems, Fe/S-TiO₂ was the most promising for various photocatalytic applications, such as in solar photocatalysis, pollutant degradation, water splitting, solar cells, and solar fuel production.

Supplementary Materials: The following supporting information can be downloaded at: <https://www.mdpi.com/article/10.3390/ECP2023-14699/s1>, Figure S1: Calculated cell volume differences of (a) TM-doped TiO₂ relative to pristine TiO₂ and (b) TM/S co-doped TiO₂ relative to S-doped TiO₂; Calculated density differences of (c) TM-doped TiO₂ relative to pristine TiO₂ and (d) TM/S co-doped TiO₂ relative to S-doped TiO₂; and calculated energy differences of (e) TM-doped TiO₂ relative to pristine TiO₂ and (f) TM/S co-doped TiO₂ relative to S-doped TiO₂; Figure S2: Simulated XRD profiles of various TM-doped TiO₂ systems; Figure S3: Simulated XRD profiles of various TM/S co-doped TiO₂ systems; Figure S4: Electronic structures of: (a) Fe/S-TiO₂, (b) Co/S-TiO₂, (c) Ni/S-TiO₂, (d) Cu/S-TiO₂, and (e) S-TiO₂; Figure S5: Optical absorption spectra of: (a) Fe/S-TiO₂, (b) Co/S-TiO₂, (c) Ni/S-TiO₂, (d) Cu/S-TiO₂, and (e) pristine TiO₂; Figure S6: Volcano plot of late transition metals and sulfur co-doped TiO₂; Table S1: Effects of various transition metals on the properties of TM-doped titanium dioxide; Table S2: Effects of various transition metals on the properties of TM/S co-doped titanium dioxide; Table S3: Effects of various transition metals on the crystallinity of TM-doped titanium dioxide; Table S4: Effects of various transition metals on the crystallinity of TM/S co-doped titanium dioxide.

Funding: This research received no external funding.

Institutional Review Board Statement: Not applicable.

Informed Consent Statement: Not applicable.

Data Availability Statement: The data presented in this study are available in the Supplementary Materials.

Conflicts of Interest: The author declares no conflict of interest.

References

1. Akira, F.; Kenichi, H. Electrochemical Photolysis of Water at a Semiconductor Electrode. *Nature* **1972**, *238*, 37.
2. El-Shafai, N.; El-Khouly, M.; El-Kemary, M.; Ramadan, M.; Derbalah, A.; Masoud, M. Fabrication and characterization of graphene oxide–titanium dioxide nanocomposite for degradation of some toxic insecticides. *J. Ind. Eng. Chem.* **2019**, *69*, 315–323. [[CrossRef](#)]
3. Suhadolnik, L.; Pohar, A.; Novak, U.; Likožar, B.; Mihelič, A.; Čeh, M. Continuous photocatalytic, electrocatalytic and photo-electrocatalytic degradation of a reactive textile dye for wastewater-treatment processes: Batch, microreactor and scaled-up operation. *J. Ind. Eng. Chem.* **2019**, *72*, 178–188. [[CrossRef](#)]
4. Lin, W.; Xie, X.; Wang, X.; Wang, Y.; Segets, D.; Sun, J. Efficient adsorption and sustainable degradation of gaseous acetaldehyde and o-xylene using rGO-TiO₂ photocatalyst. *Chem. Eng. J.* **2018**, *349*, 708–718. [[CrossRef](#)]
5. Shu, Y.; Ji, J.; Xu, Y.; Deng, J.; Huang, H.; He, M.; Leung, D.; Wu, M.; Liu, S.; Liu, S.; et al. Promotional role of Mn doping on catalytic oxidation of VOCs over mesoporous TiO₂ under vacuum ultraviolet (VUV) irradiation. *Appl. Catal. B* **2018**, *220*, 78–87. [[CrossRef](#)]
6. Sansotera, M.; Kheyli, S.G.M.; Baggioli, A.; Bianchi, C.; Pedferri, M.; Diamanti, M.; Navarrini, W. Absorption and photocatalytic degradation of VOCs by perfluorinated ionomeric coating with TiO₂ nanopowders for air purification. *Chem. Eng. J.* **2019**, *361*, 885–896. [[CrossRef](#)]
7. Pennington, A.; Yang, R.; Munoz, D.; Celik, F. Metal-free hydrogen evolution over defect-rich anatase titanium dioxide. *Int. J. Hydrogen Energy* **2018**, *43*, 15176–15190. [[CrossRef](#)]

8. Krysiak, O.; Barczuk, P.; Bienkowski, K.; Wojciechowski, T.; Augustynski, J. The photocatalytic activity of rutile and anatase TiO₂ electrodes modified with plasmonic metal nanoparticles followed by photoelectrochemical measurements. *Catal. Today* **2019**, *321–322*, 52–58. [[CrossRef](#)]
9. Taherinia, M.; Nasiri, M.; Abedini, E.; Pouretedal, H. Comparing the photocatalytic activity of N-doped and S-doped titanium dioxide nanoparticles for water splitting under sunlight radiation. *J. Iran. Chem. Soc.* **2018**, *15*, 1301–1310. [[CrossRef](#)]
10. Henderson, M. A surface science perspective on TiO₂ photocatalysis. *Surf. Sci. Rep.* **2011**, *66*, 185–297. [[CrossRef](#)]
11. Nguyen, C.; Juang, R. Efficient removal of cationic dyes from water by a combined adsorption-photocatalysis process using platinum-doped titanate nanomaterials. *J. Taiwan Inst. Chem. Eng.* **2019**, *99*, 166–179. [[CrossRef](#)]
12. Genova-Koleva, R.; Alcaide, F.; Álvarez, G.; Cabot, P.; Grande, H.-J.; Martínez-Huerta, M.; Miguel, O. Supporting IrO₂ and IrRuO nanoparticles on TiO₂ and Nb-doped TiO₂ nanotubes as electrocatalysts for the oxygen evolution reaction. *J. Energy Chem.* **2019**, *34*, 227–239. [[CrossRef](#)]
13. Rajabi, M.; Abrinaei, F. High nonlinear optical response of Lanthanum-doped TiO₂ nanorod arrays under pulsed laser irradiation at 532 nm. *Opt. Laser Technol.* **2019**, *109*, 131–138. [[CrossRef](#)]
14. Kumar, S.; Devi, L. Review on modified TiO₂ photocatalysis under UV/visible light: Selected results and related mechanisms on interfacial charge carrier transfer dynamics. *J. Phys. Chem. A* **2011**, *115*, 13211–13241. [[CrossRef](#)]
15. Meng, Q.; Wang, T.; Liu, E.; Ma, X.; Ge, Q.; Gong, J. Understanding electronic and optical properties of anatase TiO₂ photocatalysts co-doped with nitrogen and transition metals. *Phys. Chem. Chem. Phys.* **2013**, *15*, 9549–9561. [[CrossRef](#)] [[PubMed](#)]
16. Song, K.; Han, X.; Shao, G. Electronic properties of rutile TiO₂ doped with 4d transition metals: First-principles study. *J. Alloys Compd.* **2013**, *551*, 118–124. [[CrossRef](#)]
17. Liu, X.; Li, Y.; Wei, Z.; Shi, L. A Fundamental DFT Study of Anatase (TiO₂) Doped with 3d Transition Metals for High Photocatalytic Activities. *J. Wuhan Univ. Technol. Mater. Sci. Ed.* **2018**, *33*, 403–408. [[CrossRef](#)]
18. Peighambardoust, N.; Asl, S.K.; Mohammadpour, R.; Asl, S. Bandgap narrowing and electrochemical properties in N-doped and reduced anodic TiO₂ nanotube arrays. *Electrochim. Acta* **2018**, *270*, 245–255. [[CrossRef](#)]
19. Mahmoud, M.; Akhtar, M.; Mohamed, I.; Hamdan, R.; Dakka, Y.; Barakat, N. Demonstrated photons to electron activity of S-doped TiO₂ nanofibers as photoanode in the DSSC. *Mater. Lett.* **2018**, *225*, 77–81. [[CrossRef](#)]
20. Ma, Y.; Fu, J.; Tao, X.; Li, X.; Chen, J. Low temperature synthesis of iodine-doped TiO₂ nanocrystallites with enhanced visible-induced photocatalytic activity. *Appl. Surf. Sci.* **2011**, *257*, 5046–5051. [[CrossRef](#)]
21. He, Z.; Zhan, L.; Hong, F.; Song, S.; Lin, Z.; Chen, J.; Jin, M. A visible light-responsive iodine-doped titanium dioxide nanosphere. *J. Environ. Sci.* **2011**, *23*, 166–170. [[CrossRef](#)] [[PubMed](#)]
22. Wu, H.; Lin, S.; Wu, J. Effects of nitrogen concentration on N-doped anatase TiO₂: Density functional theory and Hubbard U analysis. *J. Alloys Compd.* **2012**, *522*, 46–50. [[CrossRef](#)]
23. Dagherir, R.; Drogui, P.; Robert, D. Modified TiO₂ for environmental photocatalytic applications: A review. *Ind. Eng. Chem. Res.* **2013**, *52*, 3581–3599. [[CrossRef](#)]
24. DiPaola, A.; Marci, G.; Ikeda, S.; Ohtani, B.; Palmisano, L. Transition metal doped TiO₂: Physical properties and photocatalytic behaviour. *Int. J. Photoenergy* **2001**, *3*, 171–176.
25. Chauhan, N.; Singh, V.; Kumar, S.; Kumari, M.; Sirohi, K. Synthesis of nitrogen & palladium co-doped mesoporous titanium dioxide nanoparticles via evaporation induced self assembly method and study of their photocatalytic properties. *J. Mol. Struct.* **2019**, *1185*, 219–228.
26. Tbesi, I.; Benito, M.; Molins, E.; Llorca, J.; Touati, A.; Sayadi, S.; Najjar, W. Effect of Ce and Mn co-doping on photocatalytic performance of sol-gel TiO₂. *Solid State Sci.* **2019**, *88*, 20–28. [[CrossRef](#)]
27. Ratso, S.; Käärik, M.; Kook, M.; Paiste, P.; Aruväli, J.; Vlassov, S.; Kisand, V.; Leis, J.; Kannan, A.; Tammeveski, K. High performance catalysts based on Fe/N co-doped carbide-derived carbon and carbon nanotube composites for oxygen reduction reaction in acid media. *Int. J. Hydrogen Energy* **2019**, *44*, 12636–12648. [[CrossRef](#)]
28. Lopez, E.; Cleofe, V.; Cañal, R.; Boado, K.; Perez, J. Highly-Organized One-Dimensional Copper-Doped Titanium Dioxide Nanotubes for Photoelectrocatalytic Degradation of Acid Orange 52. *Key Eng. Mater.* **2019**, *801*, 285–291. [[CrossRef](#)]
29. Wang, Y.; Zhang, R.; Li, J.; Li, L.; Lin, S. First-principles study on transition metal-doped anatase TiO₂. *Nanoscale Res. Lett.* **2014**, *9*, 46. [[CrossRef](#)]

Disclaimer/Publisher's Note: The statements, opinions and data contained in all publications are solely those of the individual author(s) and contributor(s) and not of MDPI and/or the editor(s). MDPI and/or the editor(s) disclaim responsibility for any injury to people or property resulting from any ideas, methods, instructions or products referred to in the content.